BEAM INSTRUMENTATION AT THE ACCELERATOR TEST FACILITY 2

Stewart T. Boogert on behalf of the ATF2 collaboration,
John Adams Institute at Royal Holloway,
Department of Physics, Royal Holloway, Egham, TW20 0EX, UK

Abstract

The Accelerator Test Facility 2 (ATF2) is an energy scaled demonstration system for final focus beam lines of linear high energy colliders. The ATF2 requires various advanced diagnostic systems to successfully focus the 1.3 GeV ATF electron beam to a vertical beam size of 37 nm at the *interaction point* (IP). The essential beam instrumentation includes, optical transition radiation monitors (OTRs), high resolution cavity beam position monitors (CBPMs) and a beam size monitor based on Compton scattering from a laser interference pattern (IPBSM). Four OTR (Optical Transition Radiation) monitors allow the fast measurement of projected (2D) and intrinsic (4D) emittances and the coupling correction with upstream skew quadrupole magnets. Three main types of cavity BPMs are used; C-band operating at 6.426 GHz, S-band at 2.888 GHz and low-Q C-band at the focus point. The resolution of the C-band system with attenuators was approximately 250 nm (27 nm without attenuation) and 1 μm for the S-band system. The IPBSM can measure beam sizes from 6 μm down to approximately 25 nm and recently has measured beams of order 60 to 70 nm. Prototype measurement systems are also being developed at ATF2; high speed beam position and angle feedbacks, laser-wire transverse beam size measurement and high resolution OTR monitors. The laserwire and high resolution OTR use a special set of electron beam optics to generate an $\sim$ 1 μm vertical beam size with recent measurements showing a sensitivity to beams of this size.

ACCELERATOR TEST FACILITY 2

The future energy frontier electron positron colliders plan to collide particles in the hundred GeV to TeV energy range. There are two colliders in the planning and R&D phase, the International Linear Collider (ILC) [1] and Compact Linear Collider (CLIC) [2]. In order to obtain the luminosity required by the particle physics program at these facilities, there are stringent requirements on the beam emittance and focusing systems.

After acceleration the particle beams are manipulated and controlled by a final focus system (FFS) [3] . The ATF2 [4] is a test FFS built as an extension of the existing ATF injector and damping ring. Some parameters of the ATF2 compared with ILC and CLIC are shown in Table 1 and the design optics for the ATF2 lattice are shown in Figure 1.

The ATF2 has two goals, firstly to demonstrate that the 1.3 GeV ATF beam can be focused to a 37 nm vertical beam size and secondly to keep that focus stable in vertical position for extended periods of time. Another implicit goal of the ATF2 is to test the beam instrumentation systems required, primarily to achieve goals 1 and 2, but also provide a test bed for instrumentation required at ILC or CLIC. The primary elements of the ATF2 beam instrumentation required for goal 1 are, a cavity beam position monitor system, a four station optical transition radiation emittance measurement system and a laser interference pattern Compton beam size monitor. In addition to these systems additional diagnostics systems are being developed for goal 2 and for application at the final machine, including low-Q high resolution CBPMs, a laser wire Compton beam size monitor and position feedback systems which use CBPMs as input. This paper describes these systems in turn and where applicable also gives exemplars of measurements using these tools.

Table 1: ILC, CLIC and ATF2 Machine Parameters

Parameter	ILC	CLIC	ATF2
Beam Energy (E/GeV)	500	3000	1.3
Vertical emittance (ϵ_y pm.rad)	0.07	0.003	22
IP vertical beta (β_y^* mm)	0.48	0.07	0.1
IP vertical beam size (σ_y nm)	5.9	1.0	37

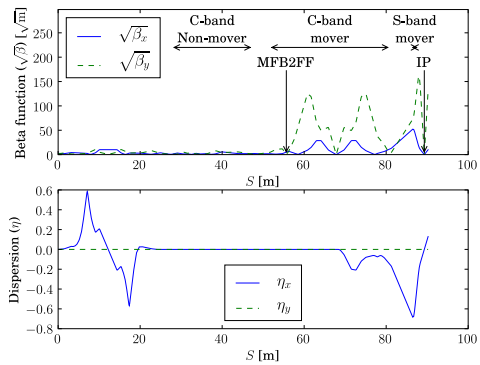

Figure 1: ATF2 design vertical and horizontal, beta and dispersion functions.

CAVITY BEAM POSITION MONITORS

The cavities utilise the position sensitive dipole mode with monopole suppressing waveguides that only extract this mode. The BPMs have 4 symmetric rectangular waveguide couplers, two for each transverse plane. There are three main CBPM types, C-band in the extraction and final focus systems, S-band located in the final doublet and

ISBN 978-3-95450-127-4

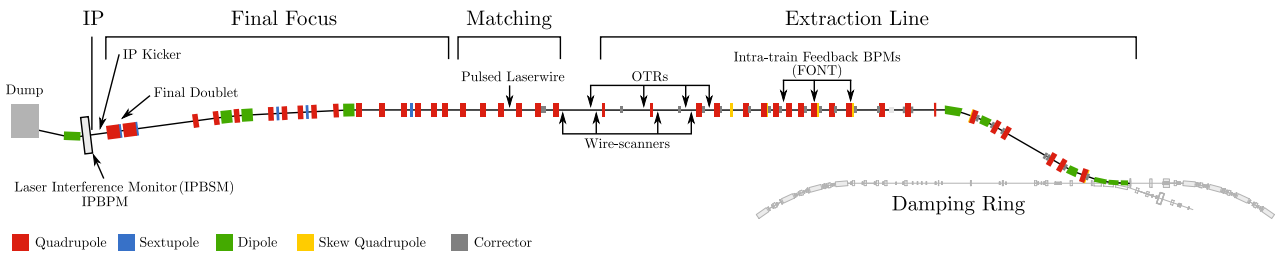

Figure 2: Plan diagram of the ATF2 accelerator facility, with the beam instrumentation marked.

IP C-band which are located just beside the IP. The main parameters of the cavities are shown in Table 2.

Table 2: Cavity BPM Parameters

Parameter	C-Band	IP C-Band y (x)	S-Band
Frequency (GHz)	6.422	6.421 (5.708)	2.888
Q_L (approximate)	6000	2100 (1300)	1800
x-y isolation (dB)	45	NA	16

Principle of Operation

The dipole CBPM voltage output $V_{\text{cavity}}(t)$ as a function of time t for a polarisation is given by

$$V_{\text{cavity}}(t) = q\, e^{-t/\tau - i\omega t}(S_d d + S_{d'} d' e^{\pi i/2} + S_\theta \theta e^{-\pi i/2}) \quad (1)$$

where q is the bunch charge, τ is the cavity decay time, ω is the cavity angular frequency, d is the beam displacement from the cavity centre, d' is the bunch tilt, θ is the beam angle and the S are constants of proportionality. The bunch charge and beam arrival phase is monitored using *reference* cavities utilising the monopole mode.

Electronics

The signals from the two output ports for a given direction are combined using an anti-phase hybrid. The electronics for the C- and S-band CBPMs consist of an amplification stage, single image rejection mixer downconverters and filtering with gains of 25 dB and 12 dB respectively. Most of the C-band CBPM output signals are attenuated by 20 dB to avoid saturation of the digitiser system and simplify the digital processing algorithm. The local oscillator (LO) signals for the C-band RF electronics are generated by dedicated phase locked electronics in the case of the C-band system and a low noise (but not phase locked) synthesiser for the S-band system. The intermediate frequency (IF) signals are digitised by 100 MHz Struck 8 channel, 14-bit waveform VME digitisers. The VME processor-controller publishes the waveform data through EPICS.

Signal Processing

The IF signal from the electronics V_{elec} are digitised and then mixed digitally using a complex local oscillator V_{LO} of frequency ω_{DDC} to baseband and filtered using a Gaussian time domain filter $g(t_i)$, with a bandwidth of approximately 3 MHz to remove the 2ω signal, to give a baseband signal y_{DDC}, so

$$y_{\text{DDC}} = g \otimes (V_{\text{elec}} \times V_{\text{LO}}). \quad (2)$$

The signal amplitude $A(t_i)$ and phase $\phi(t_i)$ is simply calculated in the usual way,

$$A(t_i) = \sqrt{y_{\text{DDC}}(t_i) \cdot y^*_{\text{DDC}}(t_i)} \quad (3)$$

$$\phi(t_i) = \arctan\left[\frac{\text{Im}[y_{\text{DDC}}(t_i)]}{\text{Re}[y_{\text{DDC}}(t_i)]}\right]. \quad (4)$$

The DDC LO frequency ω_{DDC} is determined by minimising the gradient of the phase of the down converted signal. For both the dipole and reference cavities the amplitude and phase are sampled at a single point and used to calculate the in-phase I and quadrature-phase Q signal of the baseband BPM signal compared with the appropriate (nearest spatially and correct frequency) reference cavity, so

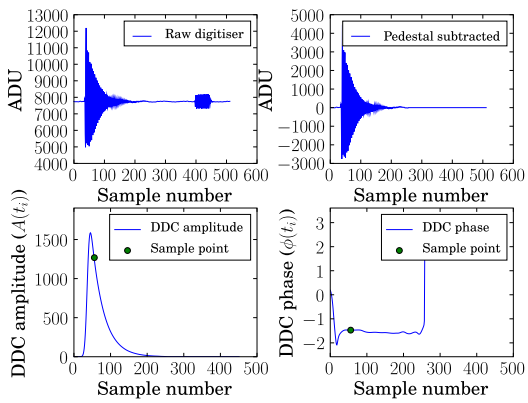

Figure 3: Example of CBPM waveform down-conversion digital signal processing.

$$I = \frac{A_d}{A_r}\cos(\phi_d - \phi_r) \quad (5)$$

$$Q = \frac{A_d}{A_r}\sin(\phi_d - \phi_r). \quad (6)$$

Figure 3 shows an example of the digital signal processing to I an Q values.

ISBN 978-3-95450-127-4

Calibration

The quadrupoles in the final focus are mounted on three axis (vertical, horizontal and roll) mover systems, elsewhere the CBPMs unmovable. Calibration is performed by moving the quadrupole which holds the BPM, or in the extraction line by performing a 4-magnet closed orbit bump and a movement of a final doublet magnet for the IP-BPMs, whilst recording the I and Q signals. Provided the move is only in position, the phase of the position signal θ_{IQ} can be determined by

$$\theta_{IQ} = \tan^{-1}\left(\frac{dQ}{dI}\right). \quad (7)$$

Rotating the I-Q phasor by θ_{IQ}, via

$$I' = I\cos(\theta_{IQ}) + Q\sin(\theta_{IQ}) \quad (8)$$
$$Q' = -I\sin(\theta_{IQ}) + Q\cos(\theta_{IQ}), \quad (9)$$

leaves I' dependent on position and Q' dependent on bunch tilt and beam trajectory. Then the I' needs to be simply scaled by a factor S to position by measuring the gradient of I' with the cavity or beam motion $y_{\rm cal}$, for example vertically,

$$\frac{1}{S_y} = \frac{dI'}{dy_{\rm cal}}. \quad (10)$$

The CBPM or beam is typically moved between ± 500 μm to ± 250 μm in both directions and the I and Q response recorded as function of beam position within the cavity. An example quadrupole mover calibration is shown in Figure 4.

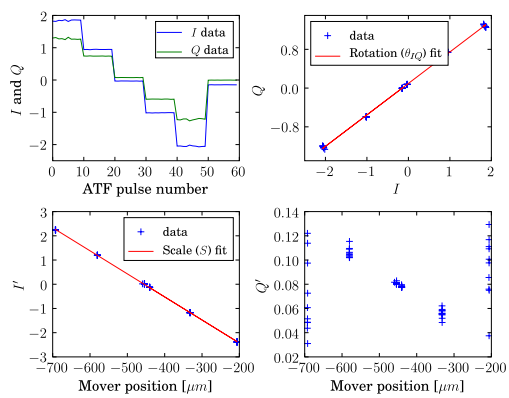

Figure 4: Example calibration of a CBPM installed on a magnet with a mover system.

System Performance and Stabililty

The resolution of the BPM system is measured using a model independent method based on singular value decomposition. The entire machine pulse of CBPMs position measurements is correlated with an individual CBPM of interest. The resulting correlation coefficients are then used to form a prediction of the beam position at the CBPM. This removes most of the beam jitter. The resolution of C-band BPMs with 20 dB attenuators using this method is typically 250 nm, without attenuators this drops to 27 nm as shown in Figure 5 [5]. The S-band system typically has resolution of 1 μm and the IP C-band BPMs is approximately 100 nm (at the IP where there is large beam divergence, previous studies have shown resolution bellow 10 nm.)

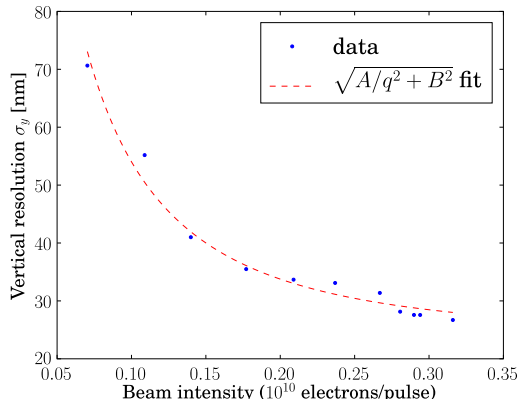

Figure 5: Vertical CBPM resolution as function of bunch charge.

To test the long term stability of the BPM system, a selection of final focus BPMs were calibrated once or twice a week for a three week period and variation of the calibration rotation and scale monitored. Typically the scales varied less than $< 1\%$, whilst the rotation was less than 4 degrees at C-band. The calibration constants were also insensitive to the movement range over which the calibration was taken, bunch charge and length [6].

INTERACTION POINT BPMS AND FEEDBACK

There are two hardware based feedback systems installed at the ATF2. These two systems are based on the Feedback on Nanosecond Times-scales (FONT) digital feedback boards. One system is a prototype system for the ILC IP feedback and located in the extraction line. This upstream feedback system uses three stripline BPMs to measure the beam which is then corrected using a fast rise time amplifier and two kickers to stabilise the ATF2 beam in position and angle. A second feedback test system for ATF2 goal 2 is located at the interaction point and uses the output from low-Q high resolution CBPMs as the input signal to a small stripline kicker [7].

OPTICAL TRANSITION RADIATION MONITORS

The OTR emittance measurement system [8] consists of 4 OTR beam size measurement devices installed in the zero design dispersion section of the extraction line, marked in Figure 2. The objective of the system is to make rapid emittance and x-y coupling measurements, using beam size

ISBN 978-3-95450-127-4

measurements with resolution of $\sim$ 2 μm. The typical beam sizes in the OTR section is 10 to 30 μm vertically and 100 to 250 μm horizontally. Figure 6 shows an individual OTR beam size monitor installed on the beam line. The small chamber is mounted on a vertical and horizontal stage system to move the chamber on to the beam axis. The targets are either 1 μm thick aluminium foil (OTR0,1) or aluminium coated kapton foil (OTR2,3). The OTR light is focused using a microscope objective lens (5X with remotely variable magnification between 3.6X and 25X) onto a Pro-sillica gigabit ethernet camera. The entire system is controlled and readout via EPICS. The magnification of the optical system is calibrated by moving the OTR stations both vertically and horizontally and the OTR centroid measured as function of mover position.

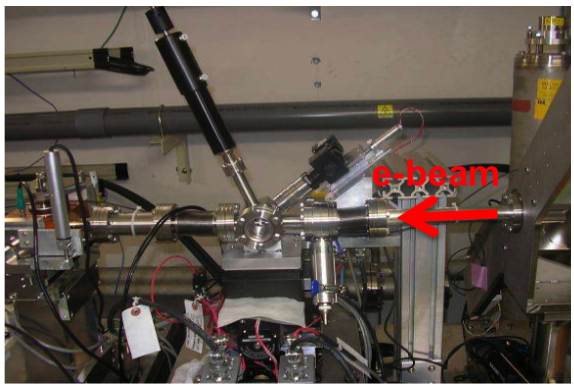

Figure 6: Photograph of an OTR monitor installation.

Figure 7 shows an example measurement of the beam profile at one of the OTR locations. The image is either projected on the x and y camera axes or a two-dimensional gaussian is fitted directly. Typically in emittance measurements 10 to 20 OTR images are taken with each OTR station and dark frame subtracted. The projected and/or intrinsic emittance measurements are compared with an online model of the ATF2 to extract the required coupling correction or provide an emittance value.

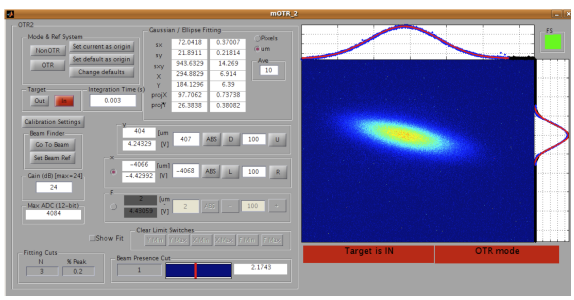

Figure 7: Example of an OTR beam size measurement.

HIGH RESOLUTION OTR

The resolution of conventional OTR beam profile monitors in the optical wavelength range is diffraction limited and defined by a root-mean square width of the point spread function (PSF). The PSF can be described as response of an optical system to a source distribution generated by a single charge. The best resolution achieved by conventional OTR monitors is about a few micrometers. However, using a method based on the analysis of the PSF visibility sub-micrometer resolution can be achieved.

This method was recently implemented in an OTR experiment [9], integrated into the laserwire experimental system. The observed vertical polarisation component of the OTR has a two-lobe structure with a clear minimum in the centre. The visibility of the distribution is very sensitive to electron beam size. Such strong dependence of the distribution can be applied to the beam size measurements at sub-micrometer level.

The minimum measured vertical beam size was 0.754$\pm$0.03 μm. This result is clearly demonstrated that method based on the analysis of the PSF structure gives an opportunity to measure the sub-micrometre beam sizes. A further improvement of the monitor can be achieved using a reflective optics to reduce aberration effects.

LASERWIRE

A laserwire is a non-invasive method of measuring the transverse size of an electron beam where a high power laser beam is focussed to a small size and scanned across the electron beam. With a relativistic electron beam, the laser photons are Compton-scattered to a high energy and travel near-parallel to the electron beam. A bend further along the accelerator separates the Compton-scattered photons and electrons, where the photons are detected. Unlike a conventional wire-scanner, the resolution of a laserwire is limited by the wavelength of light used, which is typically < 1 μm allowing a laserwire to provide greater resolution as well as avoiding damage from the electron beam. Such a diagnostic will be imperative for measuring low emittance electron and positron beams with high charge densities and short durations.

The laserwire experiment at the ATF was started in 2005 was recently moved in summer 2011 to a different point in the ATF2 lattice where a micrometre scale electron beam could be achieved. Recent results of this system [10] demonstrate high resolution measurements of the electron beam, even with a large aspect ratio beam that is conventionally thought to limit the use of a laserwire.

Setup

A seeded Q-switched Neodymium Yittrium Aluminium Garnet (Nd:YAG) laser with frequency-doubled output is used to deliver $\sim$150 mJ pulses with a wavelength of 532 nm to the laserwire interaction point at the repetition rate of the ATF2 repetition rate of 3.25 Hz. The laser pulses are σ_τ = 77 ps long and the electron bunches are σ_τ = 30 ps long. The laser is located outside the accelerator enclosure and transported into it in free-space with mirrors before being focussed by an aberration corrected radiation hard fused silica lens to the laserwire IP.

ISBN 978-3-95450-127-4

The Compton-scattered photons are detected approximately 10 m downstream immediately after a dipole magnet. The detector consists of a 4 × 4 × 0.6 cm lead plate followed by an Aerogel Cherenkov radiator of the same size, a light tight and guiding pipe and finally a shielded photo-multiplier tube. A data acquisition based system on EPICS is used to synchronously record laserwire data, cavity BPM system [5] and other ATF2 diagnostics.

The laser pulses and electron beam were synchronised for collisions using an optical transition radiation (OTR) screen mounted in the laserwire chamber [9]. The laser beam was directed below this and both the attenuated laser light and the OTR were detected in an avalanche photodiode. The laser timing was adjusted until both were overlapped. The OTR screen was also used as an alignment tool by comparing the bremsstrahlung radiation as the screen was lowered into the beam to the referenced position of the laser focus relative to the screen. This method allowed detectable collisions between the laser and the electron bunches to be found immediately.

To perform laserwire scans, the vacuum chamber was moved on a two-axis mover system. As the laserwire lens is mounted to the vacuum chamber, the laser focus therefore moves exactly as the vacuum chamber does. Optical encoder readouts provide 50 nm resolution on the chamber position.

Analysis

To deconvolve the laserwire scans, knowledge of the focussed laser spot size is required. In the case where the horizontal electron beam size is much less than the Rayleigh range (the distance over which the laser waist expands from its minimum at focus σ_o to $\sqrt{2}\sigma_o$), the laser size can be assumed to be constant and the scan is easily deconvolved when both the laser and electron beam have Gaussian profiles. However, with a large aspect ratio electron beam such as that at the laserwire location at ATF2 (∼100:1 - horizontal:vertical), the natural laser divergence from the focus across the width of the electron beam produces a non-Gaussian scan. This originates from the wider laser beam outside the focus area still interacting with the electron beam even when the focus of the laser beam is no longer in overlap with the electron beam as depicted in Figure 8. Therefore, both knowledge of the laser focussed spot size and the laser divergence is required to accurately deconvolve the laserwire scans using the full overlap integral of the measured laser propagation with the 3 dimensional Gaussian electron beam. The laser propagation is described in each axis is given by

$$\sigma(x) = \sigma_o \sqrt{1 + \left(\frac{(x - \Delta_x - x_{\sigma o})\lambda M^2}{4\pi\sigma_o^2} \right)^2} \qquad (11)$$

where σ_o is the minimum laser beam size, Δ_x the displacement of the laser focus from the electron beam, λ the wavelength of the light and M^2 the spatial quality factor. When the laser propagation is at an angle θ to the lab frame, the projection is calculated using

$$\sigma_l = \sqrt{(\sigma_{horizontal}\ \sin\theta)^2 + (\sigma_{vertical}\ \cos\theta)^2} \qquad (12)$$

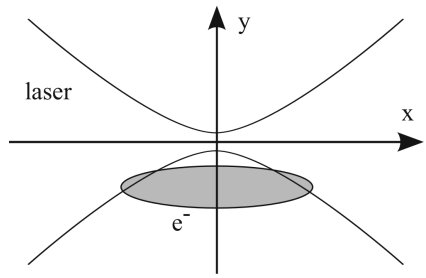

Figure 8: Schematic of laser propagation across a large aspect ratio electron beam (not to scale).

Results

The laser propagation was characterised using a larger scale focus generated by an f = 1 m plano-convex lens. A scaled focus was used as the micrometre size laser focus is beyond the measurement resolution of accurate CCD-based laser beam profilers. Beam profiles of the laser were recorded at various locations through the focus and the 4σ diameters used to fit the data to the M^2 model. This model was then scaled to the laserwire interaction focus using the measured input beam profile to the laserwire lens. The laser propagation for both axes of the laser beam is shown in Figure 9.

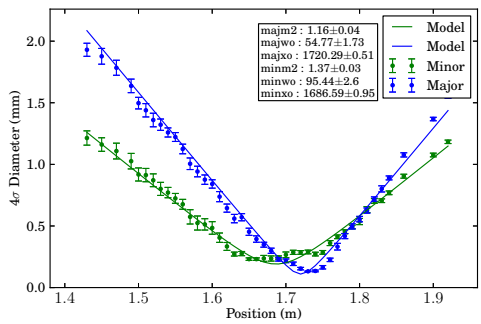

Figure 9: Measured laser propagation in both axes.

The laser propagation was found to be different in the two transverse dimensions and rotated by 17.5 ± 1.0° to the lab frame. The propagation model of each axis was used to calculate the projected vertical laser propagation in the lab frame that is relevant for deconvoluting the laserwire scans.

When performing alignment with the OTR screen, a laser machined notch in the edge of the OTR screen allowed horizontal alignment as well as vertical alignment to be performed and for the system to be aligned within 10 μm of the optimal vertical position. After the initial alignment using the OTR screen, Compton scattered photons were detectable and the collisions were then optimised.

ISBN 978-3-95450-127-4

To achieve an accurate measurement of the electron beam size, the laser focus must be centred on the electron beam, so the laserwire is first coarsely scanned vertically, then horizontally to centre the laser focus before finally performing a detailed vertical scan. The initial vertical scan is fitted to a Gaussian function, which although not an accurate description, allows the centre and approximate size to be initially determined. To deconvolve the horizontal scan using the necessary overlap integral model, knowledge of the vertical beam size is need. Similarly, to deconvolve the vertical scan, knowledge of the horizontal is needed. To overcome this circular problem, the two are fitted iteratively together until convergence is reached. The required horizontal scan of the electron beam is shown in Figure 10.

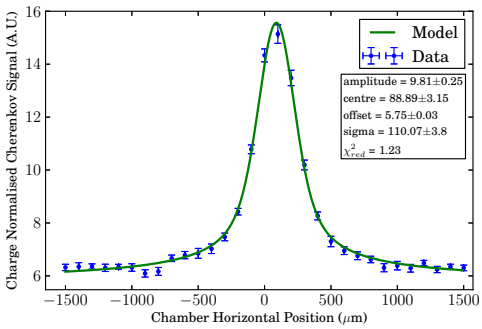

Figure 10: Horizontal scan of the electron beam.

As the divergent laser beam continues to interact with the electron beam even when the laser focus is displaced from the electron beam, the vertical laserwire scans must cover a scan range significantly greater than the vertical size of the electron beam for accurate fitting. However as the central part of the scan contains a very narrow peak, a scan with nonlinear step sizes was crucial in performing accurate laserwire scans in the minimum time possible. In Figure 11, 61 laser positions were used and 20 machine samples were recorded at each location in the vertical scan. From the iterative fitting process of both the horizontal and

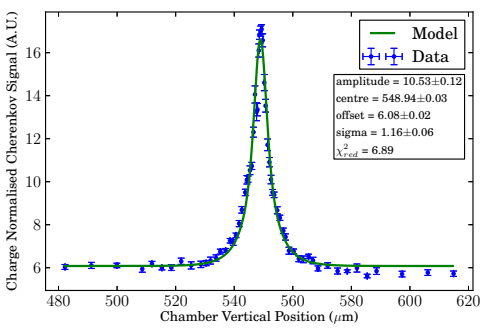

Figure 11: Detailed nonlinear vertical scan of the electron beam.

the vertical laserwire scans, the measured horizontal beam size was 110.1 $\pm$ 3.8 μm and the vertical beam size was 1.16 $\pm$ 0.06 μm.

INTERFERENCE BEAM SIZE MONITOR

Figure 12 shows a schematic of the interaction point beam size monitor (IPBSM). Unlike the laserwire the

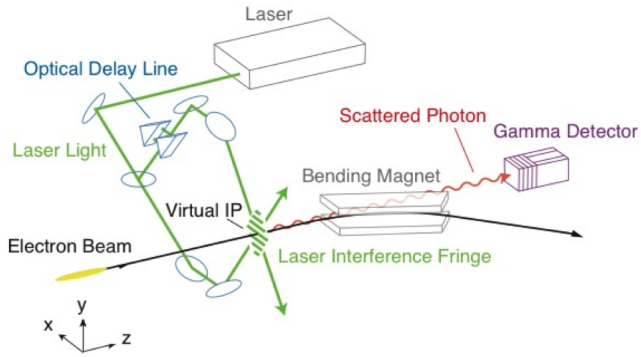

Figure 12: schematic of the IPBSM.

IPBSM forms a standing interference laser pattern around the electron beam. The bunch electrons inverse Compton scatter with laser photons producing a gamma ray signal. The laser interference fringe pattern can be moved by changing the laser path length of one of the interferometer arms. To make a beam size measurement the modulation M of the Compton signal is measured so

$$M = \frac{N_{\max} - N_{\min}}{N_{\max} + N_{\min}} = |\cos\theta| \exp\left(-2\left(k_y \sigma_y\right)^2\right) \quad (13)$$

where k_y is the vertical fringe wavenumber $k_y = \pi/d$, d is the fringe spacing $d = \lambda/(2\sin(\theta/2))$ and θ is the angle between the two interfering beams. Figure 13 shows the expected modulation as a function of electron beam size for the three IPBSM crossing angles, $2-8°$, $30°$ and $174°$

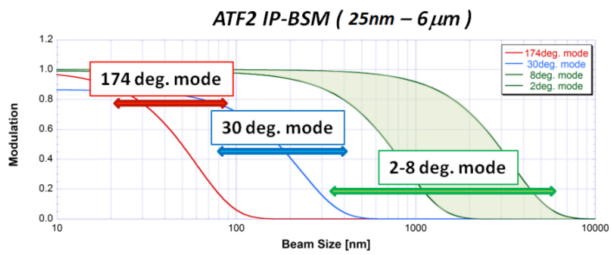

Figure 13: Compton signal modulation as function of electron beam size.

The main components of the IPBSM are; laser, optical transport and interferometer optics and Compton detector. The laser is a standard frequency doubled Nd:YAG laser, producing pulses of 1.4 J energy and 8 ns duration. The laser light is delivered to the IP via a 20 m transport optical system which also allows the adjustment of the beam size and divergence in the accelerator tunnel. The IPBSM has three permitted crossing angles, to produce interference patterns at different pitches. The IP optical system is shown

ISBN 978-3-95450-127-4

in Figure 14, the laser light can be remotely switched between the three different crossing angle optical systems mounted on a vertical optical bread board. The Compton photons are separated from the charged beam using a dipole magnet and subsequently detected using a CsI(Tl) calorimeter.

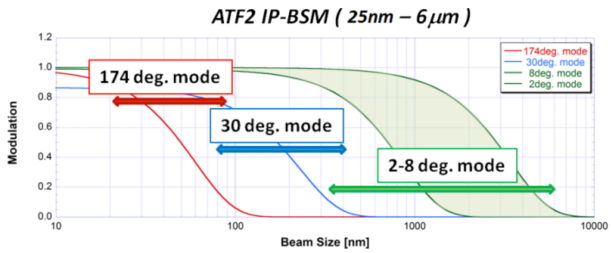

Figure 14: Photograph of the IPBSM, showing the optical system around the IP.

The IPBSM is usually operated when the electron beam has been focused to 2 μm or less, which is measured using a carbon wire scanner. The three beams are brought into coarse $\mathcal{O}(10\ \mu\mathrm{m})$ alignment using a screen which reflects laser light and also generates OTR. The waist position of each laser beam is optimised with respect to the electron focus transversely using a *laserwire* mode. Then scans of the laser focus in the electron beam direction are performed to maximise the measured fringe modulation. An example modulation measurement for $\theta = 30°$ is shown in Figure 15. As the ATF2 is tuned towards its goal of 37 nm, M

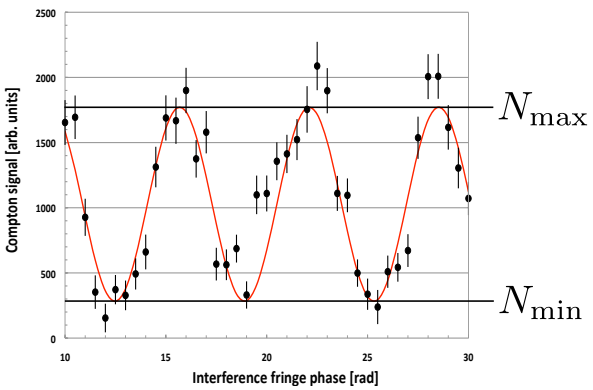

Figure 15: An example of modulation graph measured using the 30-degree mode of the IPBSM.

is continuously measured and monitored. Typically M is increased until there is no more detectable change and the IPBSM switched to larger crossing angles and this process is repeated. Recent ATF2 and IPBSM operation, in March 2013, has given modulations in the 174° mode of $M = 0.31 \pm 0.04$ giving an upper bound on the electron beam focus size of $\sigma_y = 64.9 \pm 3.5$ nm.

Systematic errors in the IPBSM system typically reduce the measured modulation, which can be parametrized as multiplicative factors C_i which must be applied to the true modulation so $M_{\mathrm{meas}} = C_1 C_2 ... M_{\mathrm{true}}$. Possible sources of systematic error include uneven laser power between the two interferometer arms, fringe rotation with respect to the beam axis, relative laser phase variation between the two arms and finally beam position variation at the IP. A more complete discussion of the systematic uncertainties in the small beam size measurement can be found in [11].

CONCLUSIONS

The ATF2 program has been successful in reaching focus beam sizes down well below 100 nm [12] and this is in part due to the excellent beam instrumentation provision. The cavity beam position monitors can perform at high resolution and stably over long periods. The multiple OTR system is used to rapidly measure the projected and intrinsic emittance and beam x-y coupling. The laserwire system has reached its design goal of being able to measure micrometer size beam sizes although this does require an ancillary horizontal beam size measurement with large electron beam aspect ratios. The IPBSM is the primary diagnostic for the focus beam size and has demonstrated beam size measurements of 65 nm on average, although this is probably an over estimation of the beam size. The first tests with fast feedback using ultra high resolution CBPMs is ongoing and is essential for achieving goal 2 of ATF2.

REFERENCES

[1] T. Behnke, J. E. Brau, B. Foster, J. Fuster, M. Harrison, *et al.*, "The International Linear Collider Technical Design Report - Volume 1: Executive Summary", (2013), arXiv:1306.6327 [physics.acc-ph].

[2] M. Aicheler, P. Burrows, M. Draper, T. Garvey, P. Lebrun, *et al.*, "A Multi-TeV linear collider based on CLIC technology: CLIC Conceptual Design Report", CERN-2012-007

[3] P. Raimondi, A. Seryi, Phys.Rev.Lett. **86**, 3779 (2001).

[4] B. I. Grishanov, *et al.*, (ATF2 Collaboration), ATF2 Proposal, SLAC-R-796, (2005).

[5] Y. I. Kim, *et al.*, Phys. Rev. ST Accel. Beams, **15** (4), 042801 (2012)

[6] S. T. Boogert, *et al.*, in proceedings of IBIC2013, Oxford, UK, MOPC27

[7] M. R. Davis, *et al*, in proceedings of IBIC2013, Oxford, UK, WEBL2

[8] A. Faus-Golfe, *et al*, in proceedings of IPAC2013, Shanghai, China, MOPWO023.

[9] K. Kruchinin, *et al.*, in proceedings of IBIC2013, Oxford, UK, WEAL2.

[10] L. Nevay, *et al.* in proceedings of IBIC2013, Oxford, UK, MOPF16.

[11] J. Yan, *et al.*, in proceedings of EAAC2013, Isola d'Elba, Italy. To be published in Nuc Instrum Meth A.

[12] G. R. White, *et al.*, "Experimental validation of a novel compact focusing scheme for future energy frontier linear lepton colliders", submitted to Phys. Rev. Lett.

ISBN 978-3-95450-127-4